Electronic structure and stability of hexagonal $Ba_3Ti_2RuO_9$

G. Radtke,[1,*] C. Maunders,[2] A. Saúl,[3] S. Lazar,[4] H. J. Whitfield,[5] J. Etheridge,[5] and G. A. Botton[2]
[1]*Institut Matériaux Microélectronique Nanosciences de Provence, UMR 6242 CNRS, Faculté des Sciences de Saint-Jérôme, Université Paul Cézanne-Aix Marseille III, Case 262, 13397 Marseille Cedex 20, France*
[2]*Canadian Centre for Electron Microscopy, McMaster University, Hamilton, Ontario, Canada L8S 4L8*
[3]*Centre Interdisciplinaire de Nanoscience de Marseille, UPR 3118 CNRS, Campus de Luminy, Case 913, 13288 Marseille Cedex 9, France*
[4]*FEI Electron Optics, Eindhoven, The Netherlands*
[5]*Monash Centre for Electron Microscopy, Monash University, Clayton, Victoria, Australia*
(Received 23 September 2009; revised manuscript received 7 January 2010; published 18 February 2010)

We investigated the electronic structure and stability of the hexagonal perovskite $Ba_3Ti_2RuO_9$ using high-resolution electron energy loss spectroscopy and first-principles band structure calculations. The comparison between experimental and theoretical results leads to a coherent picture of the electronic structure of this compound where both Ti and Ru ions are tetravalent, the first unoccupied states being of Ru 4*d* character. Structural relaxations performed on four variants of this compound allowed a detailed investigation of the influence of the Ru atoms location in the hexagonal unit cell and clarified the origin of the stabilization of this phase at room temperature. Two structures without inversion symmetry built, respectively, with two $TiRuO_9$ units (space group $P6_3mc$, 186) or with one Ru_2O_9 and one Ti_2O_9 unit ($P\bar{6}m2$,187) are found to be the most stable. The stabilization of the first structure occurs through the polarization of the partially filled Ru 4*d* bands, whereas a direct metal-metal bonding interaction taking place between the two Ru atoms in the Ru_2O_9 unit lowers the total energy of the second. The influence of the exchange correlation functional used to perform these calculations on the relative stability of the four variants is discussed.

DOI: 10.1103/PhysRevB.81.085112 PACS number(s): 79.20.Uv, 61.66.Fn, 71.20.Ps

I. INTRODUCTION

The phases of the perovskite system (ABO_3) are commonly identified by the arrangement of the AO_3 layers, which can stack in an either cubic (*c*) or hexagonal (*h*) configuration or some combination of the two. The B atoms occupy O octahedral voids between the AO_3 layers forming BO_6 octahedra. Pure *h* stacking results in columns of face-sharing BO_6 octahedra while pure *c* stacking results in BO_6 octahedra all linked by common vertices. The particular combination of *c* and *h* stacking, or polytype, adopted depends upon a number of factors such as the relative ionic radii of the constituent elements, the charge and electronic configuration of the B site cations and the particular synthetic conditions employed.

The work presented here consists in an experimental and theoretical investigation of the atomic and electronic structure of the hexagonal perovskite $Ba_3Ti_2RuO_9$. The parent structure for this compound is the six layers (6H) hexagonal $BaTiO_3$ (Fig. 1) described in the $P6_3/mmc$ (194) space group and identified by the stacking sequence $(hcc)_2$.[1,2] At room-temperature barium titanate adopts a tetragonal structure. Upon heating it undergoes a displacive phase transition to a cubic structure at 120 °C and then a reconstructive phase transition to the 6H hexagonal structure at around 1430 °C.[3] The hexagonal unit cell contains six $BaTiO_3$ formula units, the six Ti atoms occupying two cystallographically inequivalent positions. Four Ti atoms are located in Ti_2O_9 units made of pairs of TiO_6 octahedra sharing a face [see Fig. 1(b)] and the remaining two Ti, in corner sharing TiO_6 octahedra reminiscent of the cubic phase. They are labeled respectively fourfold and twofold sites.

Pauling's third rule, which states that cation polyhedra will share corners first, then edges and then faces would predict the hexagonal phase to be less stable at low temperature than the cubic phase, as observed experimentally. The stabilization of the hexagonal phase at high temperatures is possibly attributed to a loss of oxygen.[4] Recent studies have demonstrated that the 6H phase exhibits semiconducting behavior[5] and that single crystals can be prepared with a giant dielectric constant.[6] Thus, stabilizing the 6H phase at room temperature has been a focal point of the research on hexagonal $BaTiO_3$. Glaister and Kay[7] report two methods by

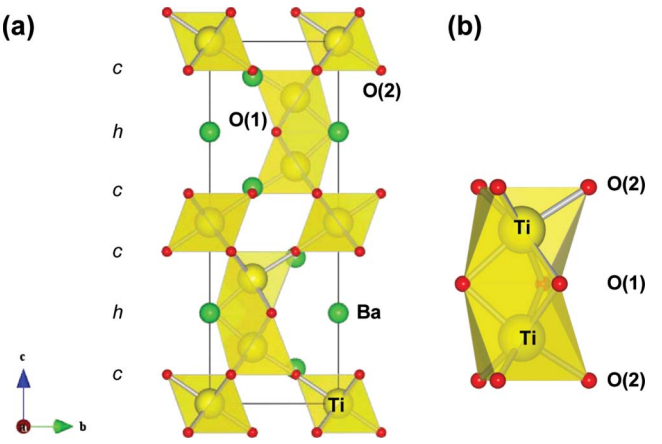

FIG. 1. (Color online) a) Unit cell of hexagonal $BaTiO_3$ in $[2\bar{1}\bar{1}0]$ orientation. Indicated is the cubic (*c*) and hexagonal (*h*) stacking of BaO_3 layers and shaded (yellow) Ti centered and O octahedra. (b) Ti_2O_9 face-sharing octahedral unit showing the crystallographically inequivalent O(1) and O(2) sites.

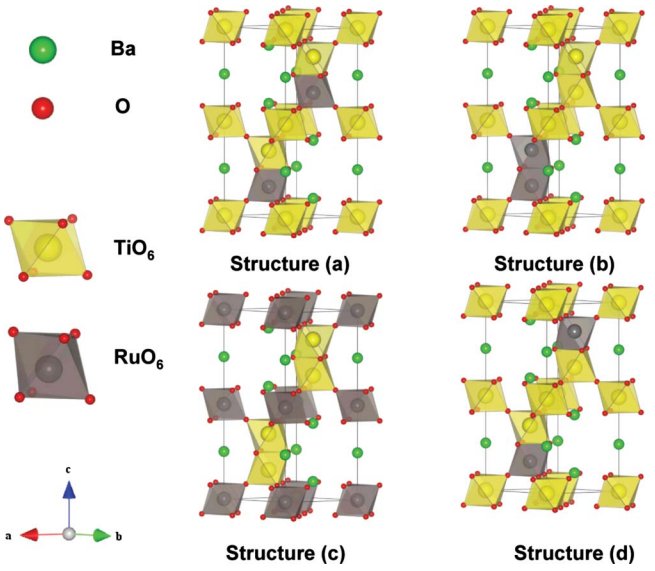

FIG. 2. (Color online) Unit cells of the four possible models (described in the text) of hexagonal $Ba_3Ti_2RuO_9$ investigated in the DFT calculations. The yellow and gray atoms represent, respectively, the Ti and the Ru atoms in their coordination octahedron. The Ba atoms are represented in green and the O atoms in red.

which the 6H structure can be stabilized at room temperature. The first involves firing in a reducing atmosphere and the second, doping the Ti site with transition metals (TM). Dickson *et al.*[4] demonstrated that a range of 3*d*, 4*d*, and 5*d* TM's, M=$Ti^{(3+)}$, V, Cr, Mn, Fe, Co, Ru, Rh, Ir, and Pt, encourage the formation of the 6H structure at room temperature, particularly for the stoichiometry $Ba_3(M,Ti_2)O_9$.

In the majority of the above compounds the M atoms preferentially occupy one of the Ti sites in the Ti_2O_9 unit thus forming a $MTiO_9$ unit. This observation naturally suggests that the interaction of the M atom at the fourfold sites with the neighboring Ti and O atoms is related to the stabilizing mechanism. In a $MTiO_9$ unit, the M cation is in close proximity to the Ti cation as a result of the face-sharing configuration and thus a strong overlap between the M-Ti (t_{2g}) *d* orbitals has been proposed.[4] This M-Ti bond is suggested to supply enough energy to override the electrostatic repulsive force between the M and Ti cations thus stabilizing the $MTiO_9$ unit and consequently the hexagonal structure.[8–10]

Recently, two convergent beam electron diffraction (CBED) works on $Ba_3Ti_2RuO_9$ (Ref. 11) and $Ba_3Ti_2MnO_9$ (Ref. 12) have given additional experimental support to the formation of the M-Ti units. They have not only confirmed the occupation of two of the fourfold sites by Ru and Mn but have also demonstrated, that there is an explicit ordering of the Ti and M cations on the fourfold sites [see structure (a) in Fig. 2]. This specific order corresponds to a space group without inversion symmetry ($P6_3mc$).

A theoretical investigation of the stability of hexagonal $Ba_3Ti_2RuO_9$ based on density functional theory (DFT) within the local spin density approximation (LSDA) has recently delivered a different conclusion.[13] The study predicted a unit cell containing one Ru_2O_9 unit and one Ti_2O_9 unit [structure (b) in Fig. 2] to be more stable than the unit cell containing two $TiRuO_9$ units [structure (a) in Fig. 2] suggested by CBED,[11] by less than 0.2 eV. The LSDA calculations suggest that the energy gain due to the interaction between the *d* electrons of the two facing Ru atoms in the Ru_2O_9 unit is strong enough to compensate the nonbonding character of the single Ti_2O_9 unit.

The aim of this work is to study the atomic, electronic, and magnetic properties of the 6H hexagonal $Ba_3Ti_2RuO_9$ in order to understand the origin of the contradiction between theoretical and experimental results on the ordering of the Ru ions in the unit cell. Here, we employed high-resolution electron energy loss spectroscopy (EELS) to probe the formal valencies of transition metals as well as the structure of the unoccupied electronic states in $Ba_3Ti_2RuO_9$. In a second part, structural relaxations performed under a DFT formalism have been carried out to probe the effect of the Ru location in the hexagonal unit cell on the total energy and magnetism of this compound. Through a systematic comparison of the results obtained within the local density approximation (LDA) and the generalized gradient approximation (GGA), we show that the apparent contradiction between experimental and theoretical results may be attributed to the failure of the former functional to describe properly the physics of $Ba_3Ti_2RuO_9$.

II. METHODS

A. Experimental details

EEL spectra were collected on a FEI 200 kV TECNAI fitted with an incident beam monochromator and a Gatan 866 spectrometer. The energy spread of the incident beam (measured at full width half maximum of the zero loss peak) was 0.1–0.2 eV. Spectra were collected in diffraction mode with a collection angle greater than 10 mrad and a dispersion of 0.05 eV/channel. The spectra presented here are a summation of individual spectra taken with an exposure time between 1 and 5 s. The individual spectra were offset from each other by 1–10 eV by varying the drift tube energy and were then manually realigned during post processing. This process allows efficient averaging of spectral noise and charge-coupled device artifacts as well as for long exposure times free from cumulative instrumental energy drift effects. The onset energy of the O K edges have been arbitrarily set to 0 eV to aid in the clarity of the display of the data.

Microcrystalline titanium oxide was prepared by hydrolysis of an isopropanol solution of titanium isopropoxide $Ti(O\,Pr^I)_4$. The dried powder was intimately mixed with stoichiometric quantities of $BaCO_3$ and RuO_2 and fired in an alumina boat in air for 24 h at 990 °C. This gave a microcrystalline product of stoichiometry $Ba_3Ti_2RuO_9$. Crystals were grown from this powder according to the method of Blattner *et al.*,[14] by heating in molten $BaCl_2$ in an alumina crucible in a tube furnace. After 72 h most of the barium chloride had evaporated and hexagonal crystal plates with basal faces up to 2 mm and of thickness less than 0.1 mm were easily separated from the remaining solidified flux by washing with water. As mentioned before, a detailed report on the crystal structure of these samples has been published recently.[11] In particular the noncentrosymmetric $P6_3mc$ space

group has been determined using CBED and the stoichiometry verified using energy dispersive x-ray spectroscopy. The lattice parameters corresponding to this phase have been measured using powder x-ray diffraction to be $a = 5.7056 \pm 0.0005$ and $c = 14.0093 \pm 0.0015$ Å.

Transmission electron microscopy samples were prepared by slightly crushing a single crystal under ethanol and cleaved fragments were allowed to settle onto a holey carbon copper grid. The grid was then placed in an oven at 80 °C to complete evaporation of the ethanol.

B. Computational details

A geometry optimization for four possible variants of the hexagonal form of $Ba_3Ti_2RuO_9$ has been conducted within both the LDA and the GGA. Assuming the absence of oxygen vacancies (see Sec. III B), these calculations investigate the influence of the Ru atoms location inside the unit cell on the structural, electronic and magnetic properties of the crystals. Starting from the parent $P6_3/mmc$ structure of hexagonal $BaTiO_3$ and replacing only the Ti with Ru atoms, four different structures, all of which having the correct stoichiometry were examined using DFT. Through a comparative examination of the total energy and the density of states (DOS) of the four structures we gained insight into the overall stabilizing mechanism. The four structures (see Fig. 2) are defined as follows. In structure (a), of space group $P6_3mc$ (186), the Ti and Ru atoms occupy alternate fourfold sites whereas the remaining Ti atoms occupy the twofold (corner sharing TiO_6 octahedral) sites. This configuration corresponds to the structure identified experimentally using CBED.[11] In structure (b), one Ru_2O_9 unit and one Ti_2O_9 unit is assumed. In this case too, the remaining Ti atoms occupy the twofold sites. The space group of the crystal is $P\bar{6}m2$ (187). In the third structure (c), two Ti_2O_9 units are assumed and the twofold sites are occupied only by Ru atoms. This structure contains an inversion center and possesses the same space group $P6_3/mmc$ (194) as hexagonal $BaTiO_3$. The fourth structure (d) resembles structure (a) in that the unit cell contains two $RuTiO_9$ units but in this structure the c glide plane is violated as the Ru-Ti ordering along the **c** axis is changed. This structure possesses the inversion symmetry and corresponds to the space group $P\bar{3}m1$ (164).

Electronic structure and total energy calculations were performed using the WIEN2K code.[15] This program is an implementation of the full-potential linearized augmented plane-wave method based on density-functional theory. The calculations presented hereafter were performed using both the local density approximation of Perdew and Wang[16] and the generalized gradient approximation of Perdew, Burke, and Ernzerhof[17] for exchange and correlation. The radii of the muffin-tin spheres were set to 2.5 a.u. for Ba, 1.85 a.u. for Ti and Ru, and 1.64 a.u. for O in all of these calculations. Relaxations of the trial structures presented in Fig. 2 were performed according to the following procedure. The total energy was computed on a grid sampling the lattice parameters a and c with a step size of 0.05 a.u. centered on the experimental lattice parameters determined by x-ray diffraction.[11] For each of these (a,c) points, a full relaxation of the internal degrees of freedom was performed. The optimal structure determined using this procedure therefore accounts for both the equilibrium lattice parameters and the equilibrium atomic coordinates inside the unit cell. These calculations were performed using a plane wave cut-off RK_{max} equal to 7 and 100 **k** points in the first Brillouin Zone, corresponding to 14 points in the irreducible wedge.

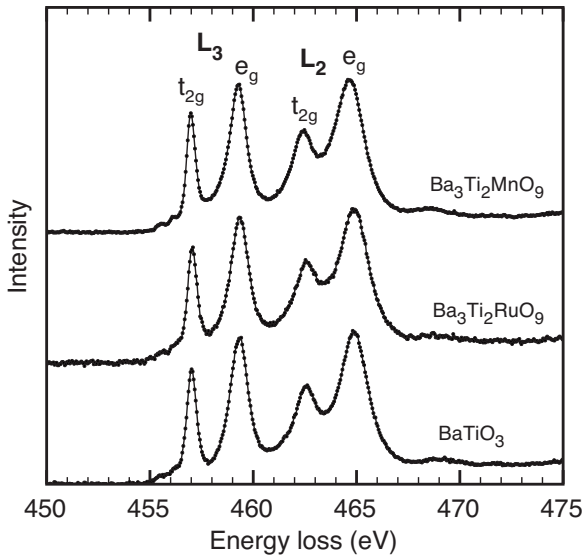

FIG. 3. Ti L_{23} edges from tetragonal $BaTiO_3$, hexagonal $Ba_3Ti_2RuO_9$, and $Ba_3Ti_2MnO_9$.

III. EXPERIMENTAL RESULTS (EELS)

A. Ti L_{23} core loss edge

The Ti L_{23} edge from $Ba_3Ti_2RuO_9$ is given in Fig. 3 along with the same edge from tetragonal $BaTiO_3$ and the isostructural compound hexagonal $Ba_3Ti_2MnO_9$.[18] The Ti L_{23} core loss edge in Ti^{4+} oxide compounds is well described by crystal-field multiplet theory assuming the local crystal-field symmetry and strength is known.[19] From an ionic perspective, Ti^{4+} has an empty $3d$ band and therefore a $2p^63d^0$ ground state configuration. Under a perfect octahedral crystal field (O_h point group symmetry), dipole excitations to the final state configuration $2p^53d^1$ yield seven permissible transitions,[20] six of which are directly observable in high-resolution EEL and x-ray absorption spectra (XAS). The four main peaks in these spectra are approximately described in a one-electron picture and can then be assigned the labels L_3: t_{2g} and e_g and L_2: t_{2g} and e_g states (as in Fig. 3). The two groups of peaks, L_3 and L_2, are separated by 3/2 times the radial factor of the $2p$ core-hole spin-orbit interaction ξ_{2p} and then the octahedral crystal field splits each group into t_{2g} and e_g components.[21] It is important to note here that a lower trigonal point group symmetry is expected in the hexagonal phase. This symmetry lowering has however no major influence on the overall shape of the edge.[22,23] The experimental Ti L_{23} edge in $Ba_3Ti_2RuO_9$ constitutes here an unambiguous signature of tetravalent Ti in octahedral coordination.

B. O K core loss edge

The O K edge EEL spectrum occurs when incident electrons lose energy in the dipole transition of a core electron in

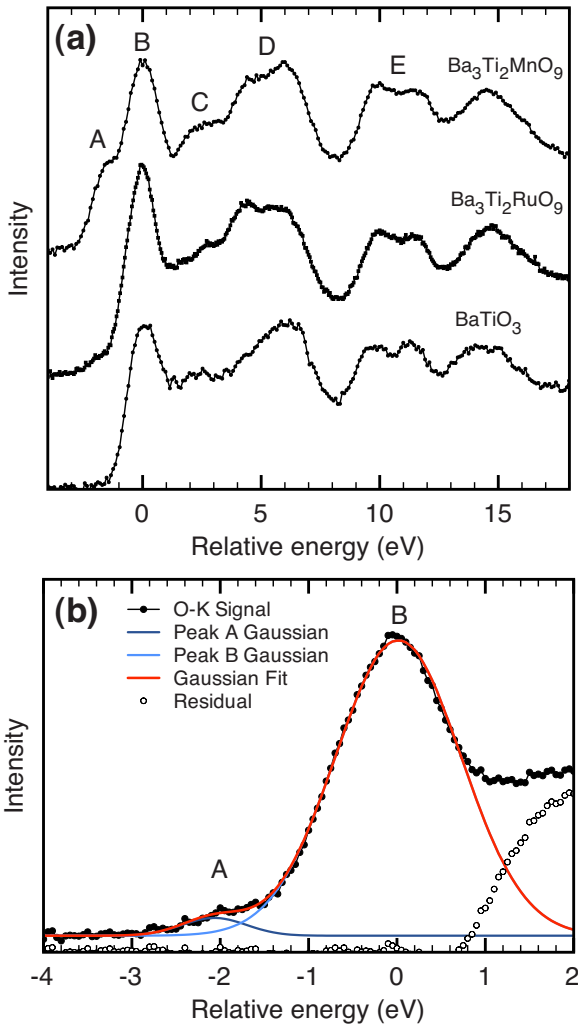

FIG. 4. (Color online) (a) O K edge from hexagonal $Ba_3Ti_2MnO_9$, hexagonal $Ba_3Ti_2RuO_9$, and tetragonal $BaTiO_3$. The evolution of a prepeak occurs in the series and an expanded view of the first 5 eV beyond the edge onset from $Ba_3Ti_2RuO_9$ is given in (b).

an atomiclike O 1*s* state to a delocalized state of O *p* character, predominately the O 2*p* states. In TM oxides, where the TM is commonly octahedrally coordinated by oxygen, the O 2*p* states are strongly hybridized with the localized TM *d* states. Therefore the fine structure, up to 5–10 eV beyond the edge onset of the O K edge contains information about the TM oxidation state, crystal field splitting and exchange energy.[24] Beyond this region and up to losses of 30 eV the features in the EEL spectra are influenced by the hybridization of the O 2*p* states with the weakly structured 4*sp* band of the TM and, in this case, the Ba 5*d* and 4*f* states (features D and E, respectively, in Fig. 4). The O K edge from $Ba_3Ti_2RuO_9$ will therefore contain information related to the hybridized Ti 3*d* and Ru 4*d*-O 2*p* states at the bottom of the conduction band and close to the edge onset while the extended region, from 5–10 eV onwards, will contain features related to high-lying Ba states.

In Fig. 4(a) the O K edge from $Ba_3Ti_2RuO_9$ is given along with the O K edges from the isostructural compound hexagonal $Ba_3Ti_2MnO_9$ (Ref. 18) and tetragonal $BaTiO_3$. As with the Ti L_{23} edges, there are only subtle differences between this series of spectra. The most striking difference between the spectra is the evolution of a prepeak or shoulder (labeled A) at the edge onset. It is absent in $BaTiO_3$, a weak feature in $Ba_3Ti_2RuO_9$ and a strong, clear feature in the spectrum acquired from $Ba_3Ti_2MnO_9$. Recent EEL work on $Ba_3Ti_2MnO_9$ attributed this feature to a state of dominant Mn 3*d* character generated in the hybridization of $Mn^{4+}(d^3)3d$ states with O 2*p* states.[18] In the same work, the structures labeled B and C, were assigned to states with Ti t_{2g} and e_g character, respectively, arising as a result of the hybridization of $Ti^{4+}(d^0)3d$ states with O 2*p* states respectively. An analogous interpretation of the O K edge in $Ba_3Ti_2RuO_9$ can be applied with the subtle difference being that the prepeak is assigned to the hybridization of the $Ru^{4+}(d^4)4d$ and O 2*p* states and has a Ru 4*d* character. The reason behind the difference in the intensity of A between $Ba_3Ti_2MnO_9$ and $Ba_3Ti_2RuO_9$ is not totally clear. It is likely a result of the different filling of the respective TM *d* band since ionically, Mn^{4+} is a d^3 cation and thus has more holes of *d* character than low spin $Ru^{4+}(d^4)$. Further, the Mn 3*d* states are more spatially localized than the Ru 4*d* states,[25] therefore leading to a narrower band of higher density of states. A prepeak at the same energy but notably higher intensity than A in $Ba_3Ti_2RuO_9$ has also been observed by others in the perovskite system $SrRu_{0.35}Ti_{0.65}O_3$.[26] In that work the prepeak was assigned to Ru 4*d* states of mainly t_{2g} character.

In Fig. 4(b) the first 5 eV of the O K edge in $Ba_3Ti_2RuO_9$ is expanded and features A and B are fitted with Gaussians so that their centroids can be assigned. The small residual confirms the accuracy of the fit and from the separation of the centroids of the Gaussians the conclusion can be made that the 4*d* states of Ru and 3*d* states of Ti are separated by approximately 2 eV, in close agreement with the value of 1.8 eV reported elsewhere.[26] An XAS study on Ru^{4+} and Ru^{5+} oxide compounds reported the Ru t_{2g} states in Ru^{5+} ($Sr_4Ru_2O_9$) to be 1 eV lower in energy than in Ru^{4+} (Sr_2RuO_4) thus making the separation from the Ti t_{2g} states close to 3 eV.[27] This value is inconsistent with the value of 2 eV we have measured and thus indirectly suggests the presence of Ru^{4+} in $Ba_3Ti_2RuO_9$, which is consistent with the stoichiometry.

IV. DENSITY-FUNCTIONAL CALCULATIONS

A. Nonmagnetic calculations

The optimized structural parameters obtained for nonmagnetic calculations in both LDA and GGA are summarized in Table I. The equilibrium lattice parameters obtained for the four different structures reproduce the experimental results within a typical error of 1% to 2%. A closer inspection of these results reveals the well-known inherent underestimation of the lattice parameters usually obtained within LDA and the slight overestimation provided by GGA functionals. When spin polarization is neglected, both approximations clearly agree in predicting (b) to be the most stable solution, well below (a), (c), and (d). As these structures only differ by the arrangement of the Ru atoms in the different octahedra,

TABLE I. Structural parameters calculated for the four trial structures of hexagonal $Ba_3Ti_2RuO_9$ relaxed in LDA and GGA. The last column shows the relative energy (in meV) per 6H unit cell. The energy of the most stable structure for each functional (LDA or GGA) is used as an energy reference (set to 0).

	Case	a (Å)	c (Å)	Metal-metal distance (Å)		Total relative energy (meV/cell)
Experiment	a	5.71	14.01			
LDA nonmagnetic	a	5.64	13.81	Ru-Ti	2.65	455
	b	5.61	13.81	Ti-Ti	2.64	0
				Ru-Ru	2.48	
	c	5.64	13.71	Ti-Ti	2.64	437
	d	5.64	13.76	Ru-Ti	2.59	480
LDA spin polarized	a	5.64	13.81	Ru-Ti	2.65	270
	b	5.61	13.81	Ti-Ti	2.64	0
				Ru-Ru	2.47	
	c	5.64	13.71	Ti-Ti	2.64	397
	d	5.64	13.81	Ru-Ti	2.60	360
GGA nonmagnetic	a	5.77	14.16	Ru-Ti	2.73	527
	b	5.74	14.13	Ti-Ti	2.69	80
				Ru-Ru	2.52	
	c	5.77	14.02	Ti-Ti	2.70	661
	d	5.77	14.08	Ru-Ti	2.66	588
GGA spin polarized	a	5.77	14.16	Ru-Ti	2.73	0
	b	5.74	14.13	Ti-Ti	2.69	3
				Ru-Ru	2.52	
	c	5.77	14.08	Ti-Ti	2.70	262
	d	5.77	14.13	Ru-Ti	2.68	206
LDA spin-polarized (previous work)[a]	a	5.67	13.90	Ru-Ti	2.67	186
	b	5.66	13.88	Ti-Ti	2.66	0
				Ru-Ru	2.49	

[a]Reference 13.

and in particular in the occupation of the face-sharing octahedral sites, one expects different local relaxations in the Ti_2O_9, Ru_2O_9, or $TiRuO_9$ units. Table I therefore includes the metal-metal distances separating the transition metal atoms located in these face-sharing coordination octahedra. As it can be seen, both Ti-Ti and Ti-Ru distances remain close to the experimental Ti-Ti (2.69 Å) distance observed in hexagonal $BaTiO_3$.[2,5] On the contrary, structure (b) exhibits a much shorter distance between the two Ru atoms present in the Ru_2O_9 structural subunit. This distance, of 2.47 and 2.52 Å in LDA and GGA, respectively, is about 6% shorter that the Ti-Ti distances observed in the other face-sharing subunit of the same unit cell. This shortening of the interatomic distance reveals a strong metal-metal interaction occurring in structure (b). This effect clearly appears when comparing the DOS of structures (a) and (b) presented in Fig. 5. In the LDA or GGA framework, the overall electronic structure of $Ba_3Ti_2RuO_9$ is constituted by a 6 eV wide valence band primarily built from the O $2p$ states and separated from the unoccupied Ti $3d$ bands by a gap of about 3 eV. The Ru $4d$ states of t_{2g} symmetry form a narrow band located in the middle of this gap. The position of the Fermi level, located in these Ru $4d$ bands, has important consequences on the relative stabilities of the different structures studied here, as we shall discuss next. This picture is coherent with the conclusions drawn from the spectroscopic results. First, the Ti $3d$ states are unoccupied and form the bottom of the conduction band therefore corresponding, in a ionic picture, to a $d^0(Ti^{4+})$ electronic configuration. Second, the Ru atoms are also formally tetravalent in this compound with their four $4d$ electrons filling two-third of the t_{2g} states, in agreement with the analysis of the O K edge. Finally, the energy separation between the unoccupied Ru $4d$ and Ti $3d$ states of t_{2g} symmetry is about 2.0 eV, in good agreement with the one observed experimentally in the O K edge between peaks A and B.

As can be seen in Fig. 5, the main difference between the DOS of structures (a) and (b) comes from these Ru-$4d$ states. Whereas they are only about 0.75 eV wide in the case of structure (a), they extend over almost 2 eV in the case of structure (b). The face-sharing octahedra in these structures are aligned along the **c** axis of the crystal with their common face in the (**a**,**b**) plane. A direct metal-metal interaction between the two Ru atoms of structure (b) would therefore essentially occur through an hybridization of the $4d$ orbitals pointing toward each other and through the common face of the coordination octahedra, i.e., primarily via the Ru d_{z^2} orbitals. Inspection of the Ru d_{z^2} local DOS clearly reveals the

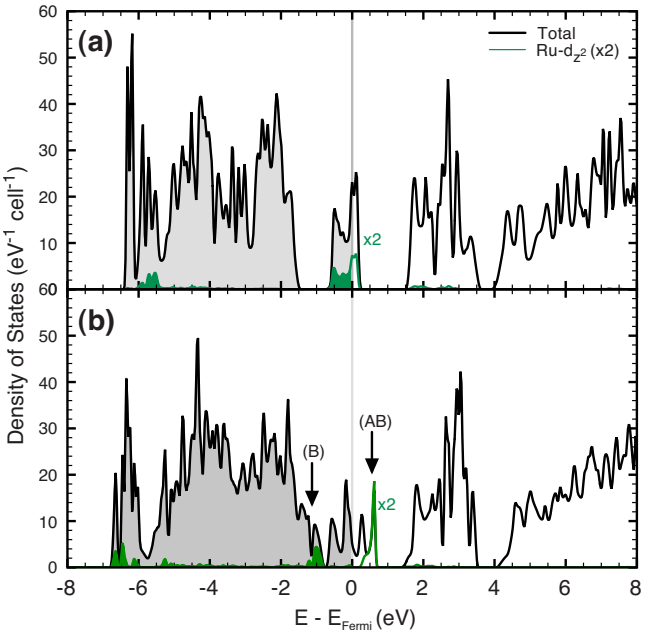

FIG. 5. (Color online) Nonmagnetic total and Ru-d_{z^2} densities of states calculated in LDA for structures (a) and (b). The bonding (b) and antibonding orbitals arising from the Ru-Ru interaction in structure (b) are indicated by the arrows. Occupied states are shaded.

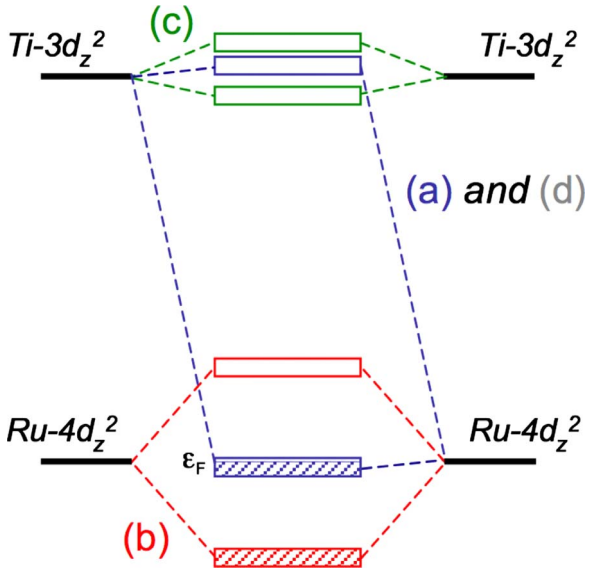

FIG. 6. (Color online) Schematic illustration of the metal-metal interaction arising from the nonmagnetic calculations in structures (a) and (d) in blue, (b) in red, and (c) in green. In case (b), the strong metal-metal interaction leads to the formation of an occupied bonding orbital and therefore, to an electronic stabilization. In cases (a), (c), and (d), the Ru-Ti or Ti-Ti interactions are negligible.

presence of such an interaction leading to the formation of localized bonding and antibonding states. Although not strictly applicable in a solid, the description of these localized states in terms of bonding and antibonding molecular orbitals arising from the interaction between the two neighboring Ru atoms seems well adapted in this case. This Ru-Ru interaction stabilizes the bonding orbital at about 1 eV below the Fermi level whereas the antibonding orbital is pushed to 0.5 eV above the Fermi level. This interaction tends to localize the electronic charge between the tetravalent Ru ions and therefore to stabilize structure (b) with respect to (a), (c), and (d) where such a strong interaction is not observed, as illustrated schematically in Fig. 6.

Nonmagnetic calculations deliver a clear picture of the chemistry taking place in these four different structures, suggesting an electronic stabilization of structure (b) associated with a direct Ru-Ru interaction. This result is in good agreement with the conclusions drawn in many other Ru-based compounds where a strong metal-metal interaction is found in DFT calculations. This is the case in $La_4Ru_6O_{19}$ where the Ru atoms are located in edge-sharing octahedral sites and where the metal-metal distance is 2.448 Å.[28,29] It is also verified in $BaRuO_3$ where the Ru atoms are also located in face-sharing octahedral sites and where the interatomic distance varies between 2.529 and 2.537 Å (Ref. 30) depending on the hexagonal polytype (4H or 9R) adopted by this compound.

An important consequence of the direct Ru-Ru interaction can be seen in the DOS presented in Fig. 5(a), where the narrow Ru-4*d* bands induce a high density of states at the Fermi level $n(E_F) \simeq 25$ states/eV in cases (a), (c), and (d). The situation is totally different for structure (b) where $n(E_F) \simeq 2$ states/eV is an order of magnitude lower. The high density of states at the Fermi level observed for (a), (c), and (d) suggests that these structures are susceptible to magnetic instability according to the Stoner criterion $In(E_F) > 1$, where I is the Stoner exchange parameter. For Ru, with an estimated value of I close to 0.6 eV (Ref. 31) this condition is largely verified for (a), (c), and (d) but it is in the limiting border for (b).

B. Spin-polarized calculations

Structural relaxations have been conducted in spin-polarized LDA and GGA for structures (a)–(d). As expected from the previous discussion, stable magnetic solutions have been found in cases (a), (c), and (d) in both LDA and GGA as summarized in Table I. Both functionals agree in predicting a much larger stabilization of structures (a), (c), and (d) where the Ru^{4+} atoms appear in the low-spin $(t_{2g\uparrow})^3(t_{2g\downarrow})^1$ state with two unpaired 4*d* electrons as shown for structure (a) in Fig. 7. On the contrary, we were unable to converge a magnetic solution for structure (b) in LDA and only a small stabilization of 80 meV/cell has been found through spin polarization in GGA (see Fig. 8 for a schematic diagram showing the relative energies of the four different structures). The difference between the two functionals can be explained by the strong variations of the DOS visible close to the Fermi level in Fig. 5 for structure (b). The slight differences in the equilibrium interatomic distances predicted in LDA and GGA induce a slightly higher DOS at the Fermi level in GGA which opens the possibility for a stable spin-polarized solution.

Although the structural parameters obtained in spin-polarized calculations (Table I) are very similar to the ones

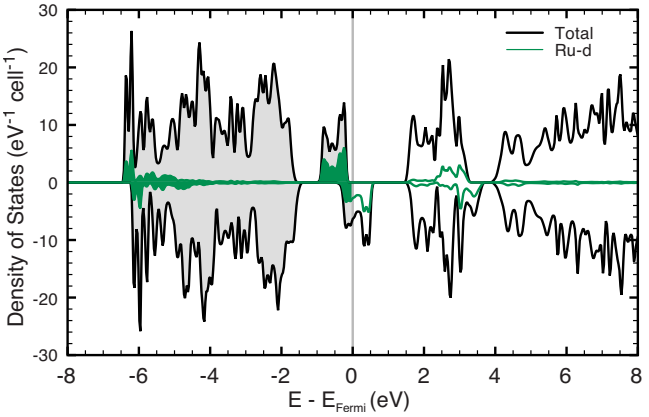

FIG. 7. (Color online) Total and Ru-*d* densities of states calculated in spin-polarized LDA for structure (a). Occupied states are shaded.

obtained in nonmagnetic calculations, large differences are found in the total energies as can be seen in Fig. 8. LDA results still predict structure (b) to be the most stable even in the absence of spin polarization. The energy gain found for structures (a), (c), and (d) is not sufficient to compete with the large electronic stabilization occurring in (b) through the Ru-Ru interaction. The situation is totally different in GGA calculations where a large stabilization of structures (a), (c), and (d) occurs through Ru-4*d* states polarization. These differences in the energy ordering of structures (a)–(d) provided by LDA and GGA find a simple explanation when considering the tendency of LDA to underestimate experimental lattice parameters and interatomic distances whereas GGA tends to slightly overestimate them. Indeed, in LDA the electronic stabilization associated with the direct Ru-Ru interaction in (b) is increased and at the same time, the energy gained through the spin polarization of the Ru-4*d* states is lowered. LDA therefore favors structure (b). These results are in good agreement with the previous calculations performed on structure (b) using a pseudopotential and plane-wave approach[13] but in clear contradiction with the CBED results.[11] In GGA, the electronic stabilization of (b) is weaker and the spin polarization leads to a larger stabilization of (a), (c), and (d). In this case, structures (a) and (b) are degenerate in energy and appear as two equally probable configurations.

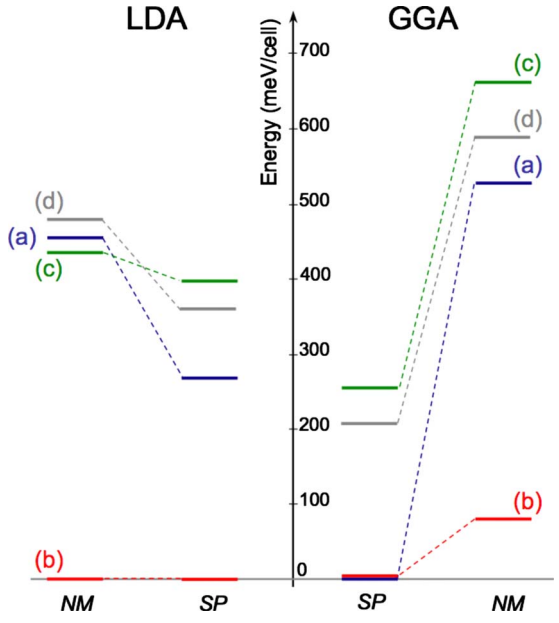

FIG. 8. (Color online) Total energy per 6H unit cell of the optimized structures calculated in both nonmagnetic and spin-polarized LDA (left) and GGA (right) approximations. For each functional, the energy of the most stable structure is taken as the energy reference.

V. DISCUSSION

We will now focus our discussion on some important aspects of the structural data resulting from the spin-polarized GGA calculations. In Table II, a summary of the O-O distances is given for the four structural models. The distances between oxygen atoms located in the same (**a**,**b**) plane are given first, a distinction being made for the fourfold site between the distance $d^{11}_{(a,b)}$ between O(1) atoms forming the face shared by the TM coordination octahedra and $d^{22}_{(a,b)}$ between O(2) atoms forming the opposite face (see Fig. 1). The distance between oxygen atoms belonging to adjacent (**a**,**b**) planes is denoted $d^{12}_{(c)}$ for the fourfold sites and $d^{22}_{(c)}$ for the twofold sites. Finally the ratio $\gamma = d_{(c)}/\langle d_{(a,b)} \rangle$ is given, indicating whether the trigonal distortion leads to a compression ($\gamma < 1$) or an elongation ($\gamma > 1$) of the octahedra along the **c** axis of the crystal.

These results reveal a systematic elongation of the fourfold octahedral sites associated with a strong shortening of the $d^{11}_{(a,b)}$ distances together with a slight compression of the twofold octahedral sites. As mentioned above, this inward displacement of the O(1) atoms forming the face shared by the coordination octahedron of the TM reflects the tendency of the system to screen their strong coulombic repulsion. It should be noted here that, in agreement with the direct Ru-Ru covalent interaction observed in structure (b), the O(1)-O(1) distance is slightly larger (2.68 Å) in this case than in the case of a Ru-Ti (2.63 Å) or a Ti-Ti (2.58 Å) pair. Table III gives a summary of the Ti/Ru off-center displacements (along the **c** axis of the crystal) in their respective octahedra. The strong trigonal distortion associated to the face-sharing configuration of the fourfold sites induces a systematic displacement of the TM ions away from the face built from the O(1) atoms shared by two coordination octahedra. This effect is indeed much more pronounced in the fourfold sites than in the twofold sites, which experience a weaker trigonal distortion due to their corner sharing arrangement. This displacement is also noticeably weaker for the Ru ions.

We can now extend our discussion to the relative stabilities of the structures (a), (c), and (d) in the light of these structural parameters. First of all, structures (c) and (d) are clearly the least stable structures tested in this study. The dominant contributor to the instability of structure (c) is likely the Ti-Ti repulsion in the Ti_2O_9 units. This repulsion appears clearly through the large Ti-Ti distance (2.70 Å) associated to a *z* displacement of 0.16 Å of the Ti ions from

TABLE II. Summary of the O-O distances (Å) extracted from the structures relaxed in spin-polarized GGA and the parameter $\gamma = d_{(c)}/\langle d_{(a,b)} \rangle$ indicating whether the trigonal distortion leads to a compression ($\gamma < 1$) or an elongation ($\gamma > 1$) of the octahedra along the **c** axis of the crystal.

	d (O-O) (Å)	Ru octahedra		Ti octahedra	
Case	γ	Twofold site	Fourfold site	Twofold site	Fourfold site
a	$d^{11}_{(a,b)}$		2.63		2.63
	$d^{22}_{(a,b)}$		2.93	2.84, 2.88	2.88
	$d^{12}_{(c)}$		2.91		2.87
	$d^{22}_{(c)}$			2.81	
	γ		1.05	0.98	1.04
b	$d^{11}_{(a,b)}$		2.69		2.58
	$d^{22}_{(a,b)}$		2.89	2.85, 2.85	2.98
	$d^{12}_{(c)}$		2.90		2.87
	$d^{22}_{(c)}$			2.80	
	γ		1.04	0.98	1.05
c	$d^{11}_{(a,b)}$		2.69		2.58
	$d^{22}_{(a,b)}$	2.88, 2.88			2.58
	$d^{12}_{(c)}$				2.86
	$d^{22}_{(c)}$	2.82			
	γ	0.98			1.05
d	$d^{11}_{(a,b)}$		2.63		2.63
	$d^{22}_{(a,b)}$		2.92	2.85, 2.85	2.90
	$d^{12}_{(c)}$		2.91		2.87
	$d^{22}_{(c)}$			2.79	
	γ		1.05	0.98	1.04

the center of their octahedra away from their common face and accompanied by a strong reduction of the O(1)-O(1) distance. Considering it is the Ti_2O_9 units that destabilize hexagonal $BaTiO_3$ at room temperature, it is not surprising that placing Ru atoms on the twofold sites does not aid in stabilizing the structure.

In structure (d), two Ru atoms are placed in the fourfold sites as in structure (a). The only difference between the two structures is the relative orientation of the $TiRuO_9$ units giving rise to unit cells without [structure (a)] or with an inversion center [structure (d)]. It is thus interesting to note that in spite of the many similarities in the local environments, structure (d) has a much higher energy than structure (a) both in LDA and in GGA (see Fig. 8). The calculations for structure (a) show that in a $TiRuO_9$ unit the Ti is displaced away from the octahedron center by 0.25 Å and away from the Ru atom. Thus in structure (d), where the orientation of the $TiRuO_9$ units with respect to the **c** axis is opposite, the Ti atoms are both displaced toward the central corner sharing TiO_6 octahedron which links them. The resulting off-center displacement is reduced (0.16 Å), in agreement with the reduction of the Ru-Ti distance (2.68 Å) observed in case (d) with respect to case (a) (2.73 Å). The movement of these ions toward the central layer built from corner sharing TiO_6 octahedra induces a local compressive stress. Because in structure (a) both $TiRuO_9$ adopt the same orientation, the strain on the corner sharing TiO_6 units is reduced by allowing the Ti to be displaced within the central octahedron. The inversion symmetry of structure (d) decreases the number of internal degrees of freedom preventing this movement and the subsequent energy gain. The specific Ti/Ru ordering along the **c** axis therefore becomes a critical factor in understanding the overall stability of the structure.

In these spin-polarized GGA calculations, both structures (a) and (b) are considered quite probable since their total energies are found to be degenerate. Interestingly, the calculations predict a large gain in energy through spin polarization for structure (a), but only a small gain in the total energy for structure (b). Early experimental measurements[4] of the high-temperature magnetic susceptibility of this compound exhibit a paramagnetic behavior. The Curie-Weiss fit of the susceptibility leads to a result of 1.9 unpaired electrons per

TABLE III. Summary of the off-center Ti/Ru displacements along the z axis in the twofold and fourfold octahedral sites extracted from the structures relaxed in spin-polarized GGA.

	Ru displacement (Å)		Ti displacement (Å)	
Case	Two-fold site	Fourfold site	Twofold site	Fourfold site
a		0.07	0.10	0.25
b		0.05	0.02	0.15
c	0			0.16
d		0.12	0	0.16

Ru atom, in total agreement with the low-spin $(t_{2g\uparrow})^3(t_{2g\downarrow})^1$ state found for structure (a).

VI. CONCLUSION

In this work, we investigated the electronic structure of the 6H hexagonal perovskite $Ba_3Ti_2RuO_9$ combining high-resolution electron energy loss spectroscopy and first-principle band-structure calculations. A coherent picture is obtained from both theory and experiments where Ti and Ru ions are tetravalent. The first unoccupied states in this compound correspond to the Ru 4*d* states of t_{2g} symmetry separated by about 2 eV from the first Ti 3*d* states. The effect of the TM ordering in the hexagonal unit cell has been studied by structural relaxation of four different variants of this compound. It led to a clarification of the mechanism responsible for the stabilization of this 6H structure at low temperature. Two structures, built respectively with two $TiRuO_9$ units [labeled (a)] or with one Ru_2O_9 and one Ti_2O_9 unit [labeled (b)] are systematically competing in both LDA and GGA. The stabilization of the first structure occurs through the spin polarization of the partially filled Ru 4*d* bands whereas a direct metal-metal bonding interaction taking place between the two Ru atoms in the Ru_2O_9 unit lowers the total energy of the second. The relative strength of these two interactions strongly depends on the equilibrium interatomic distances and lattice parameters found after the structural relaxation and therefore on the exchange functional employed in the calculations. The tendency of LDA to underestimate the experimental lattice parameters favors the second structure, as already noted by Colson *et al.*,[13] in contradiction with the experimental evidences available on this compound. On the contrary, the two structures are degenerate in GGA, promoting the first structure as a plausible solution in agreement with magnetic and structural data obtained on this compound. These results suggest that the apparent contradiction between experimental and theoretical results found previously in the literature is essentially related to the failure of LDA to describe properly the physics of this compound. We also found that the specific Ti/Ru ordering along the **c** axis between the two $TiRuO_9$ subunits present in the hexagonal phase plays a crucial role on the resulting stability of this compound. In agreement with the experimental observations,[11] our calculations show that the order which lowers the total energy is the one corresponding to a unit cell lacking an inversion center.

ACKNOWLEDGMENTS

G.R. and G.A.B. acknowledge travel funding provided by the Fonds France Canada pour la Recherche and NSERC for supporting this research. A.S. would like to acknowledge A. Zappelli for his technical support.

*guillaume.radtke@im2np.fr

[1] H. Megaw, *Crystal Structures: A Working Approach* (W. B. Saunders, London, 1973), p. 290.
[2] J. Akimoto, Y. Gotoh, and Y. Oosawa, Acta Crystallogr., Sect. C: Cryst. Struct. Commun. **50**, 160 (1994).
[3] K. W. Kirby and B. A. Wechsler, J. Am. Ceram. Soc. **74**, 1841 (1991).
[4] J. G. Dickson, L. Katz, and R. Ward, J. Am. Chem. Soc. **83**, 3026 (1961).
[5] D. C. Sinclair, J. M. S. Skakle, F. D. Morrison, R. B. Smith, and T. P. Beales, J. Mater. Chem. **9**, 1327 (1999).
[6] J. Yu, P.-F. Paradis, T. Ishikawa, S. Yoda, Y. Saita, M. Itoh, and F. Kano, Chem. Mater. **16**, 3973 (2004).
[7] R. M. Glaister and H. F. Kay, Proc. Phys. Soc. Lond. **76**, 763 (1960).
[8] N. Takeuchi, S. Ishida, and N. Wakamatsu, *Memoirs of the Faculty of Engineering and Design* (Kyoto Institute of Technology, Kyoto, Japan, 1995), Vol. **43**, p. 51.
[9] P. C. Donohue, L. Katz, and R. Ward, Inorg. Chem. **5**, 339 (1966).
[10] J. B. Goodenough and J. A. Kafalas, J. Solid State Chem. **6**, 493 (1973).
[11] C. Maunders, J. Etheridge, N. Wright, and H. J. Whitfield, Acta Crystallogr., Sect. B: Struct. Sci. **61**, 154 (2005).
[12] C. Maunders, H. J. Whitfield, D. G. Hay, and J. Etheridge, Acta Crystallogr., Sect. B: Struct. Sci. **63**, 390 (2007).
[13] T. A. Colson, M. J. S. Spencer, and I. Yarovsky, Comput. Mater. Sci. **34**, 157 (2005).
[14] H. Blattner, B. Matthias, and W. Merz, Helv. Phys. Acta **20**, 225 (1947).
[15] P. Blaha, K. Schwarz, G. Madsen, D. Kvaniscka, and J. Luitz, *Wien2k, An Augmented Plane Wave Plus Local Orbitals Program for Calculating Crystal Properties*, edited by K. Schwarz (Vienna University of Technology, Vienna, Austria, 2001).
[16] J. P. Perdew and Y. Wang, Phys. Rev. B **45**, 13244 (1992).
[17] J. P. Perdew, K. Burke, and M. Ernzerhof, Phys. Rev. Lett. **77**, 3865 (1996).
[18] G. Radtke, C. Maunders, S. Lazar, F. M. F. de Groot, J. Etheridge, and G. A. Botton, J. Solid State Chem. **178**, 3426 (2005).
[19] F. M. F. de Groot, Coord. Chem. Rev. **249**, 31 (2005).
[20] F. M. F. de Groot, J. C. Fuggle, B. T. Thole, and G. A. Sawatzky, Phys. Rev. B **41**, 928 (1990).
[21] J. P. Crocombette and F. Jollet, J. Phys.: Condens. Matter **6**, 10811 (1994).
[22] F. M. F. de Groot, M. O. Figueiredo, M. J. Basto, M. Abbate, H. Petersen, and J. C. Fuggle, Phys. Chem. Miner. **19**, 140 (1992).
[23] G. Radtke, S. Lazar, and G. A. Botton, Phys. Rev. B **74**, 155117 (2006).
[24] F. M. F. de Groot, M. Grioni, J. C. Fuggle, J. Ghijsen, G. A. Sawatzky, and H. Petersen, Phys. Rev. B **40**, 5715 (1989).
[25] Y. S. Lee, J. S. Lee, T. W. Noh, Douck Young Byun, Kwang Soo Yoo, K. Yamaura, and E. Takayama-Muromachi, Phys. Rev. B **67**, 113101 (2003).
[26] J. Kim, J.-Y. Kim, B.-G. Park, and S.-J. Oh, Phys. Rev. B **73**, 235109 (2006).

[27] Z. Hu, H. von Lips, M. S. Golden, J. Fink, G. Kaindl, F. M. F. de Groot, S. Ebbinghaus, and A. Reller, Phys. Rev. B **61**, 5262 (2000).
[28] F. Abraham, J. Tréhoux, and D. Thomas, Mater. Res. Bull. **12**, 43 (1977).
[29] P. Khalifah and R. J. Cava, Phys. Rev. B **64**, 085111 (2001).
[30] C. Felser and R. J. Cava, Phys. Rev. B **61**, 10005 (2000).
[31] P. Mohn, *Magnetism in the Solid State: An Introduction* Springer Series in Solid-State Sciences (Springer, Berlin, 2006) p. 134.